Inorganic Chemistry

pubs.acs.org/IC

Article

Spatial Compartmentalization of Cobalt Phosphide in P-Doped Dual Carbon Shells for Efficient Alkaline Overall Water Splitting

Santosh V. Mohite, Ruimin Xing, Bingyue Li, Sanjay S. Latthe, Yong Zhao, Xiying Li, Liqun Mao, and Shanhu Liu*

Cite This: https://dx.doi.org/10.1021/acs.inorgchem.9b03363

Read Online

ACCESS | Metrics & More | Article Recommendations | Supporting Information

Downloaded via MACQUARIE UNIV on January 16, 2020 at 10:42:13 (UTC).
See https://pubs.acs.org/sharingguidelines for options on how to legitimately share published articles.

ABSTRACT: Highly durable and earth-abundant bifunctional catalysts with low cell voltage are desirable for alkaline overall water splitting in the industrial fields. Herein, a novel carbon-based CoP hybrid with spatial compartmentalization of CoP nanoparticles (NPs) in P-doped dual carbon shells is achieved via a cheap Co−glycerate-template strategy. Benefitted from the uniform atomic blending of Co^{2+} ions in the Co−glycerate precursors, CoP NPs *in situ* formed in the confined space with NaH_2PO_2 as phosphorus source during the annealing process; meanwhile, glycerate suffered carbonization and transformed into P-doped dual carbon shells during the annealing process, including interior thin carbon coating, closely encircled CoP NP, and peripheral hollow carbon sphere loading a lot of CoP NPs. Not only does spatial compartmentalization of CoP NPs avoid the aggregation and expose more active sites but also P-doped dual carbon shells improve the conductivity and durability of the catalyst. As expected, the optimized hybrid exhibits outstanding electrocatalytic activities in alkaline media, such as hydrogen evolution reaction (HER) overpotential of 101 mV, oxygen evolution reaction (OER) overpotential of 280 mV, and a low cell voltage of 1.66 V to deliver a current density of 10 mA cm^{-2}. Moreover, durability and stability are greatly improved under harsh electrochemical conditions. The current strategy shades new insight into the development of carbon-based transition metal phosphides (TMP) catalysts for electrocatalysis applications.

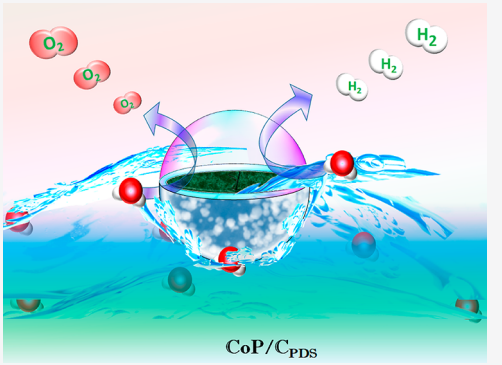

1. INTRODUCTION

Considering the environmental issues and depletion of fossil fuels, there is an urgent need to search an alternative energy carrier, which can be clean, renewable, and portable. Water electrolysis is one of the promising methods employed for the generation of highly pure hydrogen gas (H_2) and oxygen (O_2) without carbon emission via direct splitting of water molecules.[1−6] However, the substantial energy consumption cannot be ignored due to the sluggish reaction kinetics of hydrogen evolution reaction (HER) and oxygen evolution reaction (OER), which generally requires high overpotential. As known, the efficiency of hydrogen production via electrochemical water splitting is highly dependent on electrocatalysts, which are expected to afford high current at low overpotentials. Considering that, alkaline water electrolysis is more popular due to the lost-cost,[7−9] highly durable and earth-abundant bifunctional catalysts with low overpotentials are desirable in the industrial fields.

Among various nonprecious metal-based electrocatalysts such as metal oxides,[10] chalcogenides.[11−13] carbides,[14] and phosphides.[15−17] TMPs have become a hot spot for overall water splitting due to their hydrogenase-like properties. As known, phosphors atoms with more electronegativity as proton carriers can easily capture protons onto the surface of the catalyst and transfer the electrons from metal sites to the P sites, boosting the HER performance,[18] while forming peroxide intermediate to improve the OER activities.[19] Furthermore, TMPs catalysts have good electrical conductivity compared to metal oxide catalysts.[20−22] However, the poor durability and stability under harsh electrochemical conditions greatly hinder their practical applications. For example, the easy agglomeration of TMP NPs under long-term operation led to the decline of exposed active sites, thus the poor catalytic properties.[23,24] Remarkable advances have been achieved by the development of various carbon-based TMP nanocomposites to retain the catalytic activity and enhance their durability under harsh electrochemical conditions.[20,21,25,26] Besides this, many hierarchical ternary TMPs have been prepared for efficient hydrogen evolution reaction.[27,28] For example, hierarchical bimetallic Ni−Co−P microflowers with ultrathin nanosheet arrays have been prepared via a three-step method, in which the unique porous core−shell structure gives rise to

Received: November 16, 2019

© XXXX American Chemical Society

Scheme 1. Schematic Illustration for CoP NPs Encapsulated in P-Doped Dual Carbon Shells

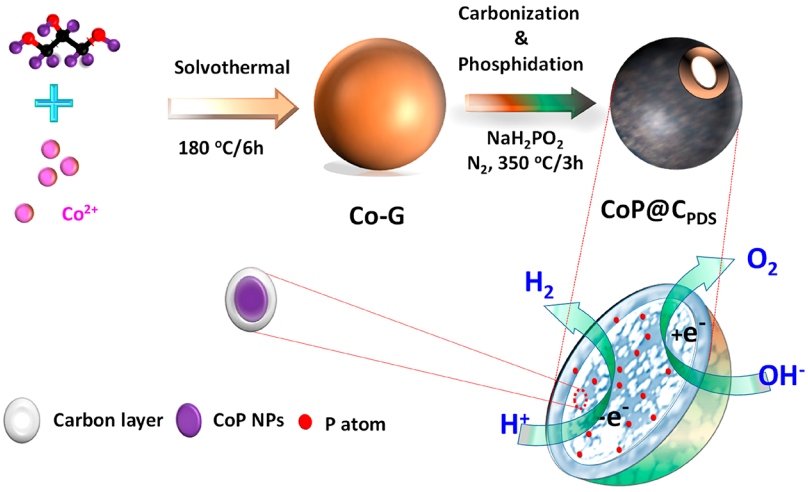

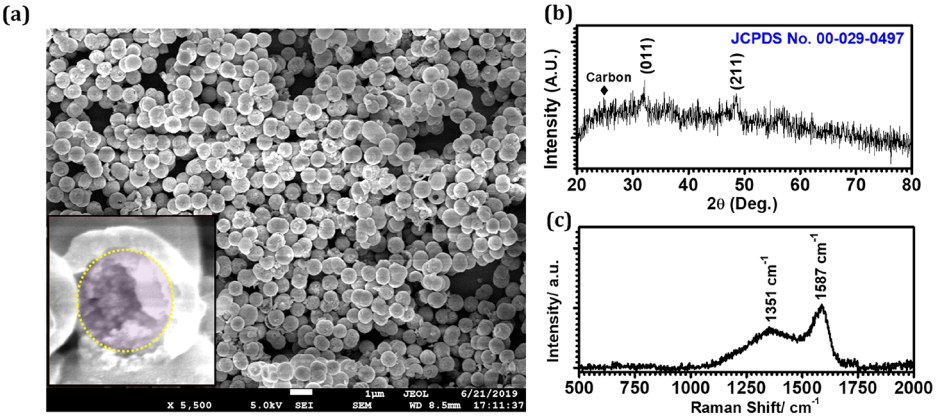

Figure 1. SEM images (a), XRD patterns (b), and Raman spectra (c) of CoP/C_{PDS}.

affluent mass transfer channels while ultrathin nanosheets offer abundant active sites, showing excellent HER performance in a wide pH range. However, cost-effective carbon-based TMPs as bifunctional electrocatalysts at low overpotentials are still challenging and rarely reported, which are beneficial to large-scale commercialization.

Motivated by the above-mentioned outstanding works, herein, a kind of novel carbon-based CoP hybrid is achieved via a cheap Co−glycerate-template strategy. With excessive NaH_2PO_2 as phosphorus source, CoP NPs were spatially compartmented by Co−glycerate precursors under annealing treatment; more interestingly, glycerate simultaneously suffered carbonization and transformed into P-doped dual carbon shells during the annealing process, including interior thin carbon coating closely encircled CoP NP and peripheral hollow carbon sphere loading a lot of CoP NPs, which were proven by HRTEM images. These P-doped dual carbon shells coated CoP NPs are denoted as CoP/C_{PDS}, which not only effectively prevent the aggregation of CoP NPs and expose more active sites but also improve the conductivity and durability of the catalyst during the harsh electrochemical measurements. As expected, the electrocatalytic activities and stability are improved.

2. EXPERIMENTAL SECTION

2.1. Chemicals. Isopropyl alcohol (IPA, 99%) and glycerol (99%), $Co(NO_3)_2{\cdot}6H_2O$, NaH_2PO_2 (99%), thioacetamide, Nafion, ethanol, and other chemicals were used as received without further purification.

2.2. Synthesis of Co−Glycerate (Co−G). The Co−glycerate solid spheres were synthesized by one-step solvothermal process according to a previous literature.[29] Typically, 0.02 mol/L of $Co(NO_3)_2{\cdot}6H_2O$ was dissolved into 20 mL of 2-propanol (IPA) under magnetic stirring at room temperature. Afterward, 4 mL of glycerol was added into the above solution to form a transparent pink solution. The obtained solution was transferred into a Teflon-lined stainless-steel autoclave and performed at 180 °C for 6 h. The obtained products were centrifuged, washed with ethanol, and dried overnight at 60 °C. The obtained cobalt glycerate precursor was abbreviated as Co−G.

2.3. Synthesis of CoP/C_{PDS}, CoP_{NS}, and Co_3O_4. Two different porcelain boats separately containing NaH_2PO_2 (750 mg, upstream position) and Co−G (50 mg, downstream position) were placed in a tubular furnace for phosphorization treatment at 350 °C for 2 h under static N_2 atmosphere to obtain CoP/C_{PDS} spheres. For comparison, CoP_{NS} and Co_3O_4 were also obtained from Co−G precursor as follows. Co−G spheres were dispersed into the mixture of water and ethanol and stirred for 24 h. Afterward, the collected products were used for phosphorization reaction to obtain CoP_{NS}. Co_3O_4 was obtained via the annealing of Co−G precursor under air atmosphere at 400 °C for 3 h.

2.4. Characterizations and Electrochemical Measurements. The detailed characterization techniques have been described in Supporting Information (Materials Characterization section). All the electrochemical measurements were carried out using three electrodes configuration connected with CHI 760E electrochemical workstation. The measurements were performed at room temperature in alkaline

https://dx.doi.org/10.1021/acs.inorgchem.9b03363
Inorg. Chem. XXXX, XXX, XXX−XXX

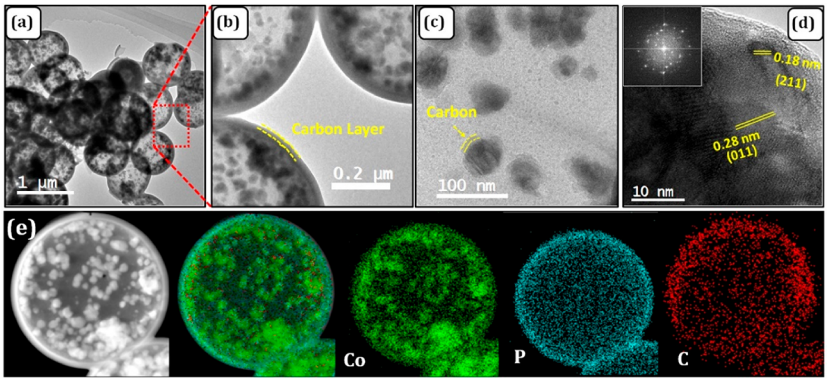

Figure 2. TEM images (a, b), HRTEM images (c, d) and elemental mapping images (e) of CoP/C_{PDS}.

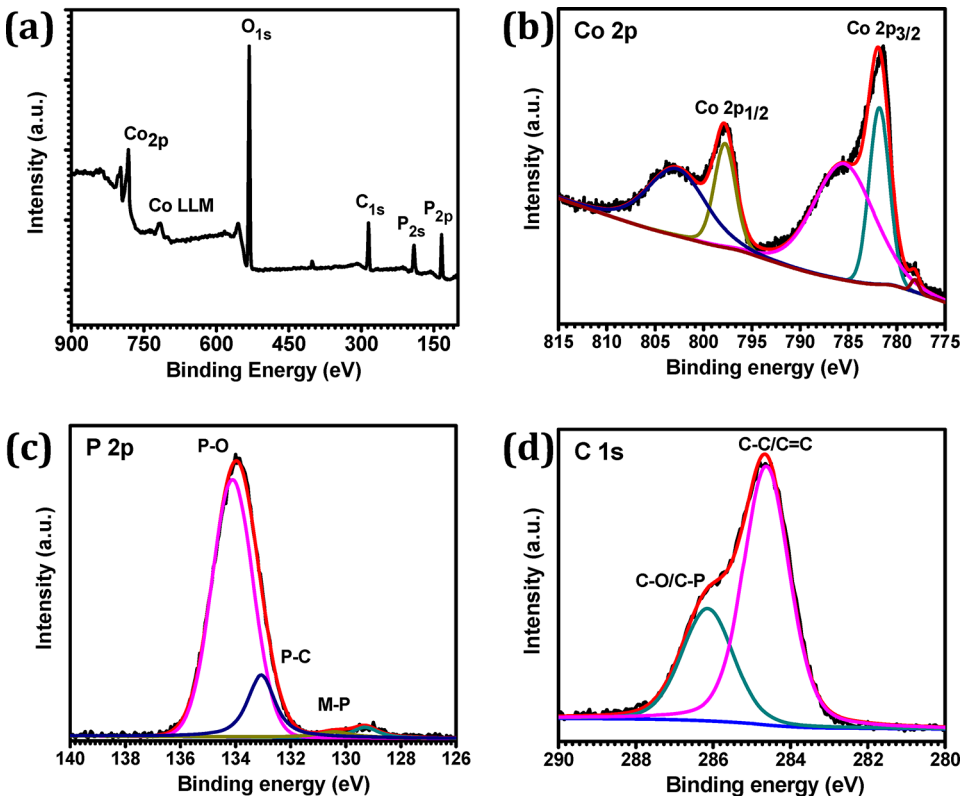

Figure 3. Survey XPS spectrum (a), high-resolution core Co 2p (b), P 2p (c), and C 1s (d) XPS spectra of CoP/C_{PDS}.

(1 M KOH) electrolyte. In electrochemical measurements, Pt wire was used as counter electrode and saturated SCE as reference electrode. All the measured potentials were calibrated with reversible hydrogen electrode (RHE) using the following equation:

$$E_{RHE} = E_{SCE} + 0.245 + 0.059 \times pH \quad (1)$$

Polarization curves for HER were recorded using linear sweep voltammetry (LSVs) technique with scan rate of 5 $mV \cdot s^{-1}$. All potentials in the LSV polarization curves were recorded without *iR*-correction. EIS analysis was carried in the frequency ranging from 10^5 to 10^{-1} Hz with an AC amplitude of 10 mV.

3. RESULTS AND DISCUSSION

The preparation illustration of CoP/C_{PDS} hybrid is shown in Scheme 1. The precursors of Co−G solid spheres are obtained via a solvothermal process. Scanning electron microscopy (SEM) image (Figure S1, Supporting Information) shows that their average diameter is 780 nm with smooth surface and XRD patterns (Figure S2, Supporting Information) indicate the noncrystalline nature. During the annealing process, the monodispersed distribution of Co^{2+} ions in the Co−G precursors ensured the formation of CoP NPs in their respective compartmentalization; meanwhile, P-doped dual carbon shells were also achieved via the carbonization of glycerate in the presence of excessive NaH_2PO_2 as phosphorus source; SEM images (Figure 1a) show that the hybrid remains the sphere-like morphologies but with rough surface and reduced diameter of 745 nm due to the shrinkage of glycerate carbonation. More specifically, a close observation from a broken CoP/C_{PDS} hybrid (marked by dotted circles) shows that the hollow carbon spheres are loaded with a lot of nanoparticles (Inset of Figure 1a). Compared with the previous reports, the preparation is quite cheap and facile; the hollow carbon spheres are expected to protect CoP NPs

https://dx.doi.org/10.1021/acs.inorgchem.9b03363
Inorg. Chem. XXXX, XXX, XXX−XXX

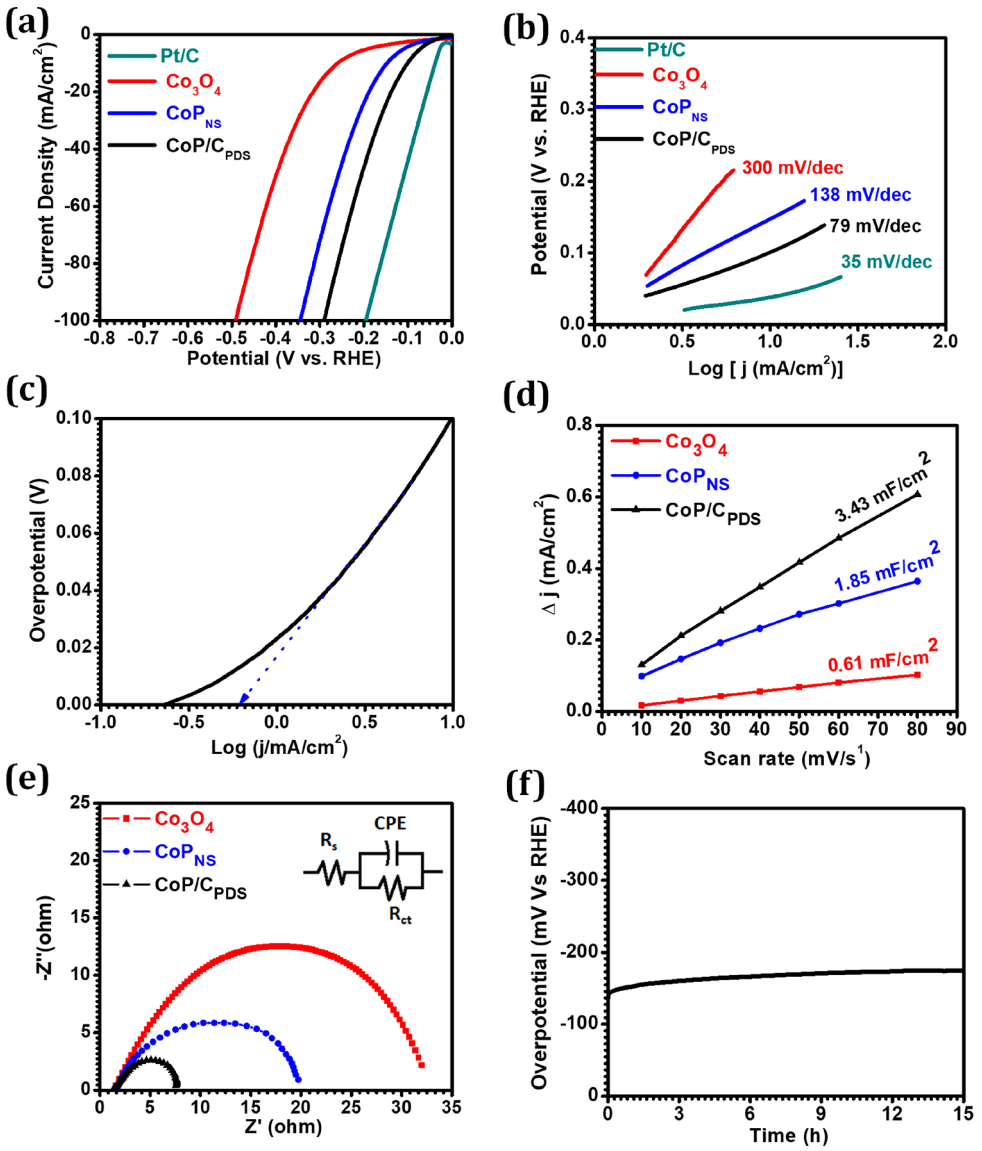

Figure 4. HER polarization curves (a), Tafel plots (b), double-layer capacitance (d), and EIS (e) of different samples in 1 M KOH; Exchange current density of CoP/C_{PDS}(c) and stability test of CoP/C_{PDS} at 20 mA cm^{-2} for 15 h with graphite rod as counter electrode (f).

from aggregation and improve the stability during the harsh electrochemical conditions.

The crystal structure of the hybrid is further investigated from XRD analysis (Figure 1b). The *d* values of diffraction peaks originated from CoP NPs are roughly matched with *d* values of the standard patterns of orthorhombic CoP crystal structure (JCPDS card no. 029−0497). Besides this, a broad peak around 25° is presumed to be the (002) reflection of amorphous carbon. The presence of amorphous carbon into the hybrid is further proven according to Raman analysis. As shown in Figure 1c, the two Raman bands are clearly visible at 1351 and 1587 cm^{-1} corresponding to G and D bands of amorphous carbon, presumably resulting from the thermolysis of organic groups in Co−G precursor.[11,30] In contrast, the XRD patterns and SEM images of Co_3O_4 and CoP_{NS} are displayed in Figure S3 and Figure S4 respectively.

Transmission electron microscopy (TEM) images (Figure 2a) further confirm that the hollow carbon spheres contain numerous monodispersed NPs with the diameter of about 36 nm. These monodispersed CoP NPs are expected to provide abundant active sites. The enlarged edge of hollow sphere (marked by the yellow line) displays the presence of amorphous carbon on the periphery of spheres (Figure 2b). The unique geometry of the hybrid (lots of NPs in hollow carbon sphere) is due to the simultaneous occurrence of carbonation and phosphorization via nanoscale Kirkendall effect, in which the internal cobalt ions diffused to the outward side faster than the external phosphorus ions diffused to the inward side during the nonequilibrium interdiffusion process at high temperature under N_2 atmospheres.[31] Therefore, the cavity formed inside the spheres. Further high-resolution TEM observation (Figure 2c and 2d) shows that numerous NPs are embraced by thin carbon shell. The lattice spacings of 0.18 and 0.28 nm clearly match with the (211) and (011) diffraction planes of CoP crystal phase; the FFT analysis (inset of Figure 2d) shows a typical polycrystalline nature of CoP NPs. Therefore, these CoP NPs with dual carbon shell protection have the potential to be free from degradation and aggregation to survive the long-term operation. The EDS of the hybrid is presented in Figure S5, in which the atomic ratio of P to Co is

https://dx.doi.org/10.1021/acs.inorgchem.9b03363
Inorg. Chem. XXXX, XXX, XXX−XXX

found to be 1.67, slightly higher than the stoichiometric composition of CoP. Furthermore, elemental mapping analysis clearly indicates that spatial distribution of Co, P, and C elements in the hybrid (Figure 2e). By contrast, carbon and phosphors are more uniformly distributed than cobalt, which suggests partial additional phosphors might be incorporated into carbon layer. Therefore, based on the above analysis, it strongly confirms that the hybrid is composed of hollow P-doped amorphous carbon spheres encapsulating thin carbon shell embraced CoP NPs.

The phosphor-doped amorphous carbon is regarded to offer remarkable benefits to improve the conductivity and catalytic activity of the electrocatalyst, not to mention the physicochemical protection for preventing active CoP NPs from degradation and aggregation.

The elemental composition of the hybrid is evaluated by using X-ray photoelectron spectroscopy (XPS). As Figure 3a shows, the survey spectrum of the hybrid indicates all the existence of P 2p, C 1s, O 1s, and Co 2p elements at 134, 285, 532, and 782 eV, respectively. The large portion of carbon suggested the carbonation of glycerate. The presence of oxygen in the hybrid is attributed to partial retention of glycerate framework and partial oxidation of catalyst surface, which exposed to the air. Deconvolution peaks of Co 2p (Figure 3b) shows that one doublet at 781.81 and 797.76 eV correspond to Co $2p_{3/2}$ and Co $2p_{1/2}$ regions, respectively, resulting from the oxidized cobalt species;[32] the two satellite peaks at 785.42 and 802.60 eV are observed in Co $2p_{3/2}$ and Co $2p_{1/2}$ regions. Besides, one small peak centered at 778.5 eV in Co $2p_{3/2}$ region is presumed to Co−P species,[33] which positively shifts by about 0.4 eV, compared to the bending energy of metallic cobalt (778.1 eV). Furthermore, deconvolution peaks of P 2p (Figure 3c) shows that one doublet at 130.38 and 129.29 eV are indexed to P $2p_{1/2}$ and P $2p_{3/2}$ of metal phosphides (M-P).[34] Compared to the binding energy of P $2p_{3/2}$ in elemental phosphorus (130.0 eV), the binding energy of P $2p_{3/2}$ in the hybrid negatively shifts by about 0.71 eV. The positive shift of metallic Co bending energy and the negative shift of elemental P bending energy give a supportive evidence of the formation of CoP and the occurrence of electron transfer from Co to P in the hybrid, which will facilitate the electrochemical reaction. In addition, the peak at 134.06 eV is assigned to phosphate species[34] (P−O bonds) due to the surface oxidation in contact with air[14] and the peak at 133.08 eV corresponds to P−C bonds, suggesting chemical interaction between carbon layer and P species, which can facilitate fast electron transfer and improve the electronic conductivity.[35] Besides that, the high-resolution C 1s XPS spectra (Figure 3d) shows two peaks at 284.60 and 286.10 eV, corresponding to the C−C/C═C, and C−O/C−P bonds, respectively.[11,36,37] Furthermore, the formation of P−C and P−O bonds are also confirmed from Fourier transform infrared spectroscopy (FT-IR), whose stretching modes are observed at 726 and 1058 cm^{-1}, respectively (Figure S6).[35,38] It is regarded that the P-doped carbon layer with lower electronegativity will play a vital role to improve the conductivity and advance water splitting.

The electrochemical analysis is used to investigate the HER performances of the hybrid catalysts in alkaline media at room temperature. As shown in Figure 4a and Figure S7, the HER activities of different catalysts and the hybrid catalysts with different weight ratios of NaH_2PO_2 to Co−G are compared. Besides, the commercial Pt/C (20 wt %) catalyst is also compared under the same conditions, which only requires a low overpotential of 38 mV at 10 mA cm^{-2}. The higher overpotentials of 260 mV and 153 mV for Co_3O_4 and CoP_{NS} catalysts are required to attain the same current density. The hybrid with the optimal ratio (NaH_2PO_2/Co−G = 15:1) give a low HER overpotential of 101 mV on foam Ni and 120 mV on glassy carbon to achieve a current density of 10 mA cm^{-2}, which is superior to the previous reported CoP-based catalysts in alkaline media, such as ultrathin CoP nanosheet aerogel[39] (154 mV), and N-doped carbon shell coated CoP nanocrystals@porous N-doped carbon substrate (165 mV).[40] The HER overpotential values of CoP-based catalyst are summarized in Table S1 with the literature survey. Although the previous reported with similar overpotentials, such a process we reported here is very cheap and controllable. Therefore, the hybrid is a promising candidate for HER electrocatalyst.[41]

The HER reaction kinetics are examined from Tafel slopes which reflect on the mass transport during the electrochemical reactions. According to the Tafel equation, it is estimated from fitting a linear portion of recorded curves and displays in Figure 4b. The state-of-the-art Pt/C electrocatalyst has ultralow values of Tafel slope (35 mV dec^{-1}), suggesting rapid kinetics. Compared with Tafel slopes of CoP_{NS} (132 mV dec^{-1}) and Co_3O_4 (300 mV dec^{-1}), Tafel slope of CoP/C_{PDS} is 79 mV dec^{-1}, which falls in the range of 40−120 mV dec^{-1}; thus, the Heyrovsky and Volmer reaction become kinetically comparable, suggesting the HER depends on the induced charge transfers during the water dissociation. The inverse ratio of Tafel slope gives the values of charge transfer coefficient.[19] The exchange current density of CoP/C_{PDS} is 0.614 mA cm^{-2} (Figure 4c), indicating high charge transfer ability for HER in alkaline media.

Besides the Tafel analysis, the utilization of catalytic active sites during electrochemical reactions is estimated from the electrochemical active surface area (ECSA) measurements, which is calculated from electrochemical double-layer capacitance (C_{dl}). The C_{dl} is determined by measuring CV curves in nonfaradaic region. The CV measurements of CoP/C_{PDS}, CoP_{NS}, and Co_3O_4 catalysts are displayed in Figure S9. The half of the slope represents the values of C_{dl} and is shown in Figure 4d. CoP/C_{PDS} has the highest values of C_{dl} compared with CoP_{NS} and Co_3O_4, which indicates that CoP/C_{PDS} provides the more electrocatalytical surface area. Therefore, the larger surface area possesses the more utilization of electroactive sites that originated from P-doped dual carbon coated CoP NPs.

In addition, the interfacial properties of catalysts highly affected on the HER performances, which is analyzed from fitting equivalent circuit. EIS measurements are performed at the same potentials of −131 mV/RHE with an amplitude of 10 mV. The semicircle nature of recorded EIS curves is used to determine the charge transfer resistance (R_{ct}). From Figure 4e, the R_{ct} values of CoP/C_{PDS}, CoP_{NS}, and Co_3O_4 are 6.40, 18.32, and 31.33 Ω respectively. The lower value of R_{ct} indicates that the designed hybrid electrocatalyst has high electrical conductivity, which is more beneficial to increase interfacial electron transfer.[37] The catalytic stability plays a crucial role for potential commercial application of catalysts, which performed by using chronopotentiometry test at a constant current density of 20 mA cm^{-2} in alkaline media. As Figure 4f shows, no recognizable decay is observed when the time-dependent stability test is recorded for 15 h, demonstrating the superior stability of CoP/C_{PDS} catalyst for HER.

https://dx.doi.org/10.1021/acs.inorgchem.9b03363
Inorg. Chem. XXXX, XXX, XXX−XXX

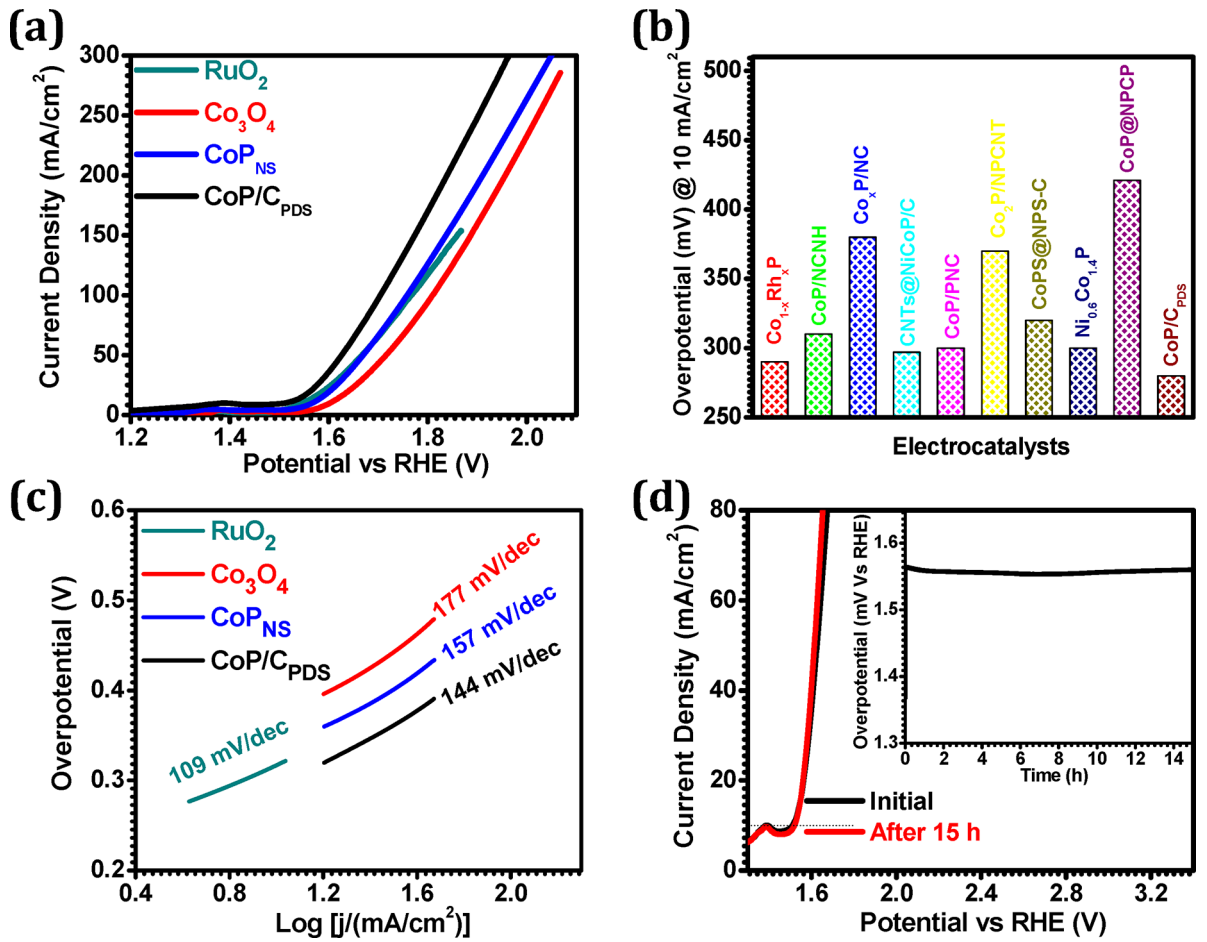

Figure 5. OER polarization curves (a), comparison of OER overpotentials (b), Tafel plots (c) of different catalysts in 1 M KOH; stability test of CoP/C_{PDS} at 20 mA cm^{-2} for 15 h (d).

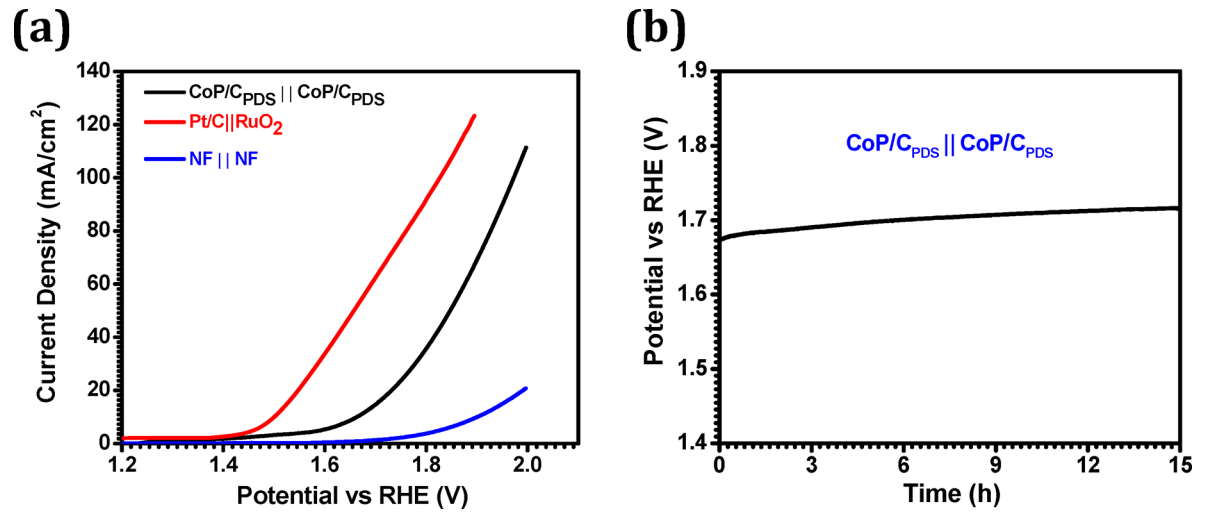

Figure 6. Polarization curves of different two-electrode cells for overall water splitting (a) and chronopotentiometric curves of CoP/C_{PDS}||CoP/C_{PDS} at 10 mA cm^{-2} in 1.0 M KOH for 15 h (b).

The OER performance of CoP/C_{PDS} catalyst as anode materials is further examined in 1.0 M KOH, together with the OER activities of CoP_{NS}, Co_3O_4, and commercial RuO_2 catalysts (industrial standard) for comparison. Polarization curves of these catalysts are recorded at a scan rate of 5 mV s^{-1} and a current density of 10 mA cm^{-2}. Figure 5a shows the CoP/C_{PDS}-modified electrode exhibits superior electrocatalytic activity with an impressive overpotential of 280 mV, compared to the state-of-the-art RuO_2 (318 mV), CoP_{NS} (337 mV), and Co_3O_4 (373 mV). Furthermore, the OER catalytic activity of CoP/C_{PDS} catalyst is remarkably superior to the ever reported CoP-based OER catalysts, such as MOF-derived Ni_2P−CoP bimetallic phosphides[15] (320 mV), polydopamine-assisted construction of cobalt phosphide NPs embedded in N-doped

https://dx.doi.org/10.1021/acs.inorgchem.9b03363
Inorg. Chem. XXXX, XXX, XXX−XXX

carbon porous polyhedrons[42] (380 mV), and CoP nanoparticles@N-doped carbon nanotube hollow polyhedron[26] (310 mV). Also, we compared with previous reported catalysts (shown in Table S2 and Figure 5b). Figure 5c gives the respective Tafel values of CoP/C_{PDS} (144 mV dec^{-1}), RuO_2 (109 mV dec^{-1}), CoP_{NS} (157 mV dec^{-1}) and Co_3O_4 (177 mV dec^{-1}), indicating that CoP/C_{PDS} has excellent electrocatalytic OER activities and better charge transfer coefficient. This superior activity is presumed from the strong integration of spatial compartmentalization of CoP NPs in P-doped dual carbon shells, which greatly enhance the charge transport at the interface. The improved stability is proven by the stability test at a constant current density of 20 mA cm^{-2}; as shown in the inset of Figure 5d, no decay in potential is observed after 15 h of continuous OER measurement, indicating CoP/C_{PDS} exhibits outstanding stability.

Considering that the superior HER and OER performances in alkaline electrolyte, the two-electrode cell with CoP/C_{PDS}||CoP/C_{PDS} as bifunctional catalysts is employed for alkaline water electrolysis test. Lots of abundant bubbles continually escape during the electrolysis, when a cell voltage of 1.66 V (corresponding to overpotential of 0.43 V) is required to achieve a current density of 10 mA cm^{-2} (Figure 6a). This result indicate the CoP/C_{PDS} catalyst coated on Ni Foam is comparable to the state-of-the-art Pt/C||RuO_2 catalysts and superior to some previous reported bifunctional catalysts at targeted current density, which summarized in Table S3. Furthermore, the durability test is evaluated at a constant current density of 10 mA cm^{-2} and shown in Figure 6b. The initial potential shows negligible changes after 15 h of long-term stability test. Therefore, the above results show that the hybrid exhibits great potential for large-scale alkaline water electrolysis with low cost and high efficiency.

CONCLUSIONS

In all, a cheap Co−glycerate-template strategy is reported as an effective method to develop space-confined phosphidation of CoP NPs in P-doped dual carbon shells. The unique geometry of the hybrid not only effectively avoids the aggregation of more active CoP NPs but also improves the conductivity and durability of the catalyst, which help the hybrid to survive the harsh electrochemical measurements. The optimal hybrid exhibits superior electrocatalytic activities in alkaline media with HER overpotential of 101 mV and OER overpotential of 280 mV at 10 mA cm^{-2}; a low cell voltage of 1.66 V is required for overall water splitting with superior durability after continuous operation for 15 h. The strategy proposed here introduces a new perspective about the development of space-confinement strategy toward highly durable and low-cost bifunctional catalysts for scale-up alkaline water electrolysis.

ASSOCIATED CONTENT

Supporting Information

The Supporting Information is available free of charge at https://pubs.acs.org/doi/10.1021/acs.inorgchem.9b03363.

Materials characterization, electrochemical measurements, SEM images, XRD patterns, EDS and IR spectra, polarization curves, CV curves, stability test, OER polarization curves, HER activity, OER activity, and full water splitting activity (PDF)

AUTHOR INFORMATION

Corresponding Author

Shanhu Liu − *Henan University, Kaifeng, P. R. China;* orcid.org/0000-0003-1382-7157; Phone: +86 0371 23881589; Email: liushanhu@vip.henu.edu.cn

Other Authors

Santosh V. Mohite − *Henan University, Kaifeng, P. R. China*

Ruimin Xing − *Henan University, Kaifeng, P. R. China*

Bingyue Li − *Henan University, Kaifeng, P. R. China*

Sanjay S. Latthe − *Henan University, Kaifeng, P. R. China;* orcid.org/0000-0002-6349-666X

Yong Zhao − *Henan University, Kaifeng, P. R. China;* orcid.org/0000-0002-5039-4576

Xiying Li − *Henan University, Kaifeng, P. R. China*

Liqun Mao − *Henan University, Kaifeng, P. R. China*

Complete contact information is available at: https://pubs.acs.org/10.1021/acs.inorgchem.9b03363

Notes

The authors declare no competing financial interest.

ACKNOWLEDGMENTS

The authors gratefully appreciate the support from the National Natural Science Foundation of China (21950410531) and Science Technology Research Project of Henan Province (182102410090). Also, we express thanks to Dr. Daibing Luo from Analytical & Testing Center of Sichuan University for the valuable discussion and characterization.

REFERENCES

(1) Hu, C.; Zhang, L.; Gong, J. Recent progress made in the mechanism comprehension and design of electrocatalysts for alkaline water splitting. *Energy Environ. Sci.* **2019**, *12*, 2620−2645.

(2) Ding, Y.; Miao, B.-Q.; Jiang, Y.-C.; Yao, H.-C.; Li, X.-F.; Chen, Y. Polyethylenimine-modified nickel phosphide nanosheets: interfacial protons boost the hydrogen evolution reaction. *J. Mater. Chem. A* **2019**, *7*, 13770−13776.

(3) Zhou, H.; Liu, K.; Li, H.; Cao, M.; Fu, J.; Gao, X.; Hu, J.; Li, W.; Pan, H.; Zhan, J.; Li, Q.; Qiu, X.; Liu, M. Recent advances in different-dimension electrocatalysts for carbon dioxide reduction. *J. Colloid Interface Sci.* **2019**, *550*, 17−47.

(4) Xue, Z.; Liu, K.; Liu, Q.; Li, Y.; Li, M.; Su, C.-Y.; Ogiwara, N.; Kobayashi, H.; Kitagawa, H.; Liu, M.; Li, G. Missing-linker metal-organic frameworks for oxygen evolution reaction. *Nat. Commun.* **2019**, *10*, 5048.

(5) Liu, A.; Liu, K.; Zhou, H.; Li, H.; Qiu, X.; Yang, Y.; Liu, M. Solution evaporation processed high quality perovskite films. *Science Bulletin* **2018**, *63*, 1591−1596.

(6) Liu, M.; Liu, M.; Wang, X.; Kozlov, S. M.; Cao, Z.; De Luna, P.; Li, H.; Qiu, X.; Liu, K.; Hu, J.; Jia, C.; Wang, P.; Zhou, H.; He, J.; Zhong, M.; Lan, X.; Zhou, Y.; Wang, Z.; Li, J.; Seifitokaldani, A.; Dinh, C. T.; Liang, H.; Zou, C.; Zhang, D.; Yang, Y.; Chan, T.-S.; Han, Y.; Cavallo, L.; Sham, T.-K.; Hwang, B.-J.; Sargent, E. H. Quantum-Dot-Derived Catalysts for CO_2 Reduction Reaction. *Joule* **2019**, *3*, 1703−1718.

(7) Chen, Z.; Duan, X.; Wei, W.; Wang, S.; Ni, B.-J. Recent advances in transition metal-based electrocatalysts for alkaline hydrogen evolution. *J. Mater. Chem. A* **2019**, *7*, 14971−15005.

(8) Anantharaj, S.; Ede, S. R.; Karthick, K.; Sam Sankar, S.; Sangeetha, K.; Karthik, P. E.; Kundu, S. Precision and correctness in the evaluation of electrocatalytic water splitting: revisiting activity

parameters with a critical assessment. *Energy Environ. Sci.* **2018**, *11*, 744−771.
(9) Wu, Z.; Wang, J.; Xia, K.; Lei, W.; Liu, X.; Wang, D. MoS_2−MoP heterostructured nanosheets on polymer-derived carbon as an electrocatalyst for hydrogen evolution reaction. *J. Mater. Chem. A* **2018**, *6*, 616−622.
(10) Bai, C.; Wei, S.; Deng, D.; Lin, X.; Zheng, M.; Dong, Q. A nitrogen-doped nano carbon dodecahedron with Co@Co_3O_4 implants as a bi-functional electrocatalyst for efficient overall water splitting. *J. Mater. Chem. A* **2017**, *5*, 9533−9536.
(11) Li, B.; Xing, R.; Mohite, S. V.; Latthe, S. S.; Fujishima, A.; Liu, S.; Zhou, Y. CoS_2 nanodots anchored into heteroatom-doped carbon layer via a biomimetic strategy: Boosting the oxygen evolution and supercapacitor performance. *J. Power Sources* **2019**, *436*, 226862.
(12) Li, S.; Zhao, S.; Xing, R.; Kumbhar, V. S.; Lee, K.; Zhou, Y.; Kazuya, N.; Fujishima, A.; Liu, S. Zn-Co-S Colloidal Nanocrystal Clusters as Efficient and Durable Bifunctional Electrocatalysts For Full Water Splitting. *ChemNanoMat* **2019**, *5*, 761−765.
(13) Liu, S.; Li, S.; Sekar, K.; Li, R.; Zhu, Y.; Xing, R.; Nakata, K.; Fujishima, A. Hierarchical ZnS@C@MoS_2 core-shell nanostructures as efficient hydrogen evolution electrocatalyst for alkaline water electrolysis. *Int. J. Hydrogen Energy* **2019**, *44*, 25310−25318.
(14) Wei, M.; Li, B.; Jin, C.; Ni, Y.; Li, C.; Pan, X.; Sun, J.; Yang, C.; Yang, R. A 3D free-standing thin film based on N, P-codoped hollow carbon fibers embedded with MoP quantum dots as high efficient oxygen electrode for Li-O2 batteries. *Energy Storage Materials* **2019**, *17*, 226−233.
(15) Liang, X.; Zheng, B.; Chen, L.; Zhang, J.; Zhuang, Z.; Chen, B. MOF-Derived Formation of Ni_2P−CoP Bimetallic Phosphides with Strong Interfacial Effect toward Electrocatalytic Water Splitting. *ACS Appl. Mater. Interfaces* **2017**, *9*, 23222−23229.
(16) Chen, L.; Zhang, Y.; Wang, H.; Wang, Y.; Li, D.; Duan, C. Cobalt layered double hydroxides derived CoP/Co_2P hybrids for electrocatalytic overall water splitting. *Nanoscale* **2018**, *10*, 21019−21024.
(17) Truong, L.; Jerng, S.-K.; Roy, S. B.; Jeon, J. H.; Kim, K.; Akbar, K.; Yi, Y.; Chun, S.-H. Chrysanthemum-Like CoP Nanostructures on Vertical Graphene Nanohills as Versatile Electrocatalysts for Water Splitting. *ACS Sustainable Chem. Eng.* **2019**, *7*, 4625−4630.
(18) Shi, Y.; Zhang, B. Recent advances in transition metal phosphide nanomaterials: synthesis and applications in hydrogen evolution reaction. *Chem. Soc. Rev.* **2016**, *45*, 1529−1541.
(19) Anantharaj, S.; Ede, S. R.; Sakthikumar, K.; Karthick, K.; Mishra, S.; Kundu, S. Recent Trends and Perspectives in Electrochemical Water Splitting with an Emphasis on Sulfide, Selenide, and Phosphide Catalysts of Fe, Co, and Ni: A Review. *ACS Catal.* **2016**, *6*, 8069−8097.
(20) Wu, F.; Chen, Z.; Wu, H.; Xiao, F.; Du, S.; He, C.; Wu, Y.; Ren, Z. In Situ Catalytic Etching Strategy Promoted Synthesis of Carbon Nanotube Inlaid with Ultrasmall FeP Nanoparticles as Efficient Electrocatalyst for Hydrogen Evolution. *ACS Sustainable Chem. Eng.* **2019**, *7*, 12741−12749.
(21) Xie, Y.; Chen, M.; Cai, M.; Teng, J.; Huang, H.; Fan, Y.; Barboiu, M.; Wang, D.; Su, C.-Y. Hollow Cobalt Phosphide with N-Doped Carbon Skeleton as Bifunctional Electrocatalyst for Overall Water Splitting. *Inorg. Chem.* **2019**, *58*, 14652−14659.
(22) Jing, Y.; Liu, H.; Yan, R.; Chen, J.; Dai, H.; Liu, C.; Zhang, X.-D. Mesoporous CoP Nanowire Arrays for Hydrogen Evolution. *ACS Applied Nano Materials* **2019**, *2*, 5922−5930.
(23) Yu, Y.; Peng, Z.; Asif, M.; Wang, H.; Wang, W.; Wu, Z.; Wang, Z.; Qiu, X.; Tan, H.; Liu, H. FeP Nanocrystals Embedded in N-Doped Carbon Nanosheets for Efficient Electrocatalytic Hydrogen Generation over a Broad pH Range. *ACS Sustainable Chem. Eng.* **2018**, *6*, 11587−11594.
(24) Zhang, X.; Yu, X.; Zhang, L.; Zhou, F.; Liang, Y.; Wang, R. Molybdenum Phosphide/Carbon Nanotube Hybrids as pH-Universal Electrocatalysts for Hydrogen Evolution Reaction. *Adv. Funct. Mater.* **2018**, *28*, 1706523.
(25) Wu, C.; Yang, Y.; Dong, D.; Zhang, Y.; Li, J. In Situ Coupling of CoP Polyhedrons and Carbon Nanotubes as Highly Efficient Hydrogen Evolution Reaction Electrocatalyst. *Small* **2017**, *13*, 1602873.
(26) Pan, Y.; Sun, K.; Liu, S.; Cao, X.; Wu, K.; Cheong, W.-C.; Chen, Z.; Wang, Y.; Li, Y.; Liu, Y.; Wang, D.; Peng, Q.; Chen, C.; Li, Y. Core−Shell ZIF-8@ZIF-67-Derived CoP Nanoparticle-Embedded N-Doped Carbon Nanotube Hollow Polyhedron for Efficient Overall Water Splitting. *J. Am. Chem. Soc.* **2018**, *140*, 2610−2618.
(27) Liu, X.; Deng, S.; Xiao, D.; Gong, M.; Liang, J.; Zhao, T.; Shen, T.; Wang, D. Hierarchical Bimetallic Ni−Co−P Microflowers with Ultrathin Nanosheet Arrays for Efficient Hydrogen Evolution Reaction over All pH Values. *ACS Appl. Mater. Interfaces* **2019**, *11*, 42233−42242.
(28) Liu, X.; Deng, S.; Liu, P.; Liang, J.; Gong, M.; Lai, C.; Lu, Y.; Zhao, T.; Wang, D. Facile self-template fabrication of hierarchical nickel-cobalt phosphide hollow nanoflowers with enhanced hydrogen generation performance. *Science Bulletin* **2019**, *64*, 1675.
(29) Ding, D.; Wang, Y.; Li, X.; Qiang, R.; Xu, P.; Chu, W.; Han, X.; Du, Y. Rational design of core-shell Co@C microspheres for high-performance microwave absorption. *Carbon* **2017**, *111*, 722−732.
(30) Ma, F.-X.; Xu, C.-Y.; Lyu, F.; Song, B.; Sun, S.-C.; Li, Y. Y.; Lu, J.; Zhen, L. Construction of FeP Hollow Nanoparticles Densely Encapsulated in Carbon Nanosheet Frameworks for Efficient and Durable Electrocatalytic Hydrogen Production. *Advanced Science* **2019**, *6*, 1801490.
(31) Xu, X.; Liu, J.; Hu, R.; Liu, J.; Ouyang, L.; Zhu, M. Self-Supported CoP Nanorod Arrays Grafted on Stainless Steel as an Advanced Integrated Anode for Stable and Long-Life Lithium-Ion Batteries. *Chem. - Eur. J.* **2017**, *23*, 5198−5204.
(32) Cao, S.; Chen, Y.; Wang, H.; Chen, J.; Shi, X.; Li, H.; Cheng, P.; Liu, X.; Liu, M.; Piao, L. Ultrasmall CoP Nanoparticles as Efficient Cocatalysts for Photocatalytic Formic Acid Dehydrogenation. *Joule* **2018**, *2*, 549−557.
(33) Tian, J.; Liu, Q.; Asiri, A. M.; Sun, X. Self-Supported Nanoporous Cobalt Phosphide Nanowire Arrays: An Efficient 3D Hydrogen-Evolving Cathode over the Wide Range of pH 0−14. *J. Am. Chem. Soc.* **2014**, *136*, 7587−7590.
(34) Ji, X.; Zhang, R.; Shi, X.; Asiri, A. M.; Zheng, B.; Sun, X. Fabrication of hierarchical CoP nanosheet@microwire arrays via space-confined phosphidation toward high-efficiency water oxidation electrocatalysis under alkaline conditions. *Nanoscale* **2018**, *10*, 7941−7945.
(35) Li, G.; Sun, Y.; Rao, J.; Wu, J.; Kumar, A.; Xu, Q. N.; Fu, C.; Liu, E.; Blake, G. R.; Werner, P.; Shao, B.; Liu, K.; Parkin, S.; Liu, X.; Fahlman, M.; Liou, S.-C.; Auffermann, G.; Zhang, J.; Felser, C.; Feng, X. Carbon-Tailored Semimetal MoP as an Efficient Hydrogen Evolution Electrocatalyst in Both Alkaline and Acid Media. *Adv. Energy Mater.* **2018**, *8*, 1801258.
(36) Gao, C.; Fang, C.; Zhao, H.; Yang, J.; Gu, Z.; Sun, W.; Zhang, W.; Li, S.; Xu, L.-C.; Li, X.; Huo, F. Rational design of multi-functional CoS@rGO composite for performance enhanced Li-S cathode. *J. Power Sources* **2019**, *421*, 132−138.
(37) Ma, J.; Wang, M.; Lei, G.; Zhang, G.; Zhang, F.; Peng, W.; Fan, X.; Li, Y. Polyaniline Derived N-Doped Carbon-Coated Cobalt Phosphide Nanoparticles Deposited on N-Doped Graphene as an Efficient Electrocatalyst for Hydrogen Evolution Reaction. *Small* **2018**, *14*, 1702895.
(38) Daasch, L.; Smith, D. Infrared Spectra of Phosphorus Compounds. *Anal. Chem.* **1951**, *23*, 853−868.
(39) Li, H.; Zhao, X.; Liu, H.; Chen, S.; Yang, X.; Lv, C.; Zhang, H.; She, X.; Yang, D. Sub-1.5 nm Ultrathin CoP Nanosheet Aerogel: Efficient Electrocatalyst for Hydrogen Evolution Reaction at All pH Values. *Small* **2018**, *14*, 1802824.
(40) Peng, Z.; Yu, Y.; Jiang, D.; Wu, Y.; Xia, B. Y.; Dong, Z. N-doped carbon shell coated CoP nanocrystals encapsulated in porous N-doped carbon substrate as efficient electrocatalyst of water splitting. *Carbon* **2019**, *144*, 464−471.

https://dx.doi.org/10.1021/acs.inorgchem.9b03363
Inorg. Chem. XXXX, XXX, XXX−XXX

(41) Yan, C.; Rosei, F. Hollow micro/nanostructured materials prepared by ion exchange synthesis and their potential applications. *New J. Chem.* **2014**, *38*, 1883−1904.
(42) Li, J.-S.; Kong, L.-X.; Wu, Z.; Zhang, S.; Yang, X.-Y.; Sha, J.-Q.; Liu, G.-D. Polydopamine-assisted construction of cobalt phosphide encapsulated in N-doped carbon porous polyhedrons for enhanced overall water splitting. *Carbon* **2019**, *145*, 694−700.

https://dx.doi.org/10.1021/acs.inorgchem.9b03363
Inorg. Chem. XXXX, XXX, XXX−XXX